Accuracy of single-shot autocorrelation measurements of petawatt laser pulses

Xiaoping Ouyang,[1,*] Jingui Ma,[2] Lin Yang,[1] Shunxing Tang,[1] Chong Liu,[1] Yonghua Peng,[1] Liejia Qian,[2] Baoqiang Zhu,[1] Jianqiang Zhu,[1] and Zunqi Lin[1]

[1]Shanghai Institute of Optics and Fine Mechanics, Chinese Academy of Sciences, No. 390, Qinghe Road, Jiading District, Shanghai 201800, China

[2]Fudan University, Shanghai 200433, China

*Corresponding author: oyxp@siom.ac.cn

Received 5 January 2012; revised 29 April 2012; accepted 29 April 2012; posted 22 May 2012 (Doc. ID 160014); published 12 June 2012

At the Shen Guang II (SGII) Petawatt Laser Facility, measurements of large-energy, single-shot laser pulses sometimes feature asymmetric autocorrelation signals, causing uncertainty in the measurement of compressed pulses. This study presents a method for defining and describing the asymmetry of autocorrelation signals. We discuss two sources of asymmetry: the nonuniform distribution of the near field excited by a beam, and the rotation of autocorrelator arms from the cylinder lens. The pulsewidth of an asymmetric autocorrelation signal is shorter than its real width. After updating the autocorrelator, the single-shot autocorrelator for the SGII petawatt laser exhibits a measurement uncertainty of below 12.3%. Recommendations on reducing asymmetry in large-energy, single-shot autocorrelation are discussed.

OCIS codes: 140.7090, 320.7080, 320.7100, 120.4640.

1. Introduction

Autocorrelation is an important and fundamental technique for diagnosing the pulsewidth of ultrashort pulses. Single-shot autocorrelation used in a high-energy laser facility enables real-time measurement. Real-time measurement is useful in fast ignition and advanced radiographic capability experiments when the compressor is adjusted. Precise measurement is crucial for calculating focused intensity. It is also an urgent requirement for the construction of a large-energy petawatt laser facility in the Shen Guang II Upgrade Program (SGII-U); the petawatt laser pulses in this facility are based on the SGII ninth beam. Ross *et al.* presented the single-shot autocorrelator for picosecond pulses. This autocorrelator had a temporal window of 15 ps by a grating's first order diffraction [1]. Collier *et al.* used a Wollaston prism and a biprism to generate two arms of a single-shot autocorrelator. This autocorrelator had a temporal window of 60 ps by a grating's second order diffraction [2]. Oba *et al.* also presented a single-shot autocorrelator with a temporal window 20 ps under transverse time delay [3]. Sack and Mourou used a single-shot autocorrelator to eliminate the pulse-front tilt of a grating compressor [4]. In recent years, single-shot autocorrelation has been developed to measure pulsewidth and contrast for SGII petawatt laser pulses [5–8]. In 2011, chirped pulses were successfully compressed to 0.58 ps in the SGII Petawatt Laser Facility, with a maximum energy of 377 J at 3.5 ps.

2. Principle of Single-Shot Autocorrelation

The measurements of large-energy, single-shot pulses in an SGII petawatt laser sometimes feature asymmetric autocorrelation signals, causing uncertainty in measuring compressed pulses. Here, we discuss this asymmetry.

1559-128X/12/183989-06$15.00/0

For a measured pulse $I(t)$, the principle of single-shot autocorrelation is

$$I_A(\tau) = \int I(t)I(t-\tau)\mathrm{d}t. \tag{1}$$

When the measured pulse is Gaussian, it can be written as

$$I(t) = I_0 \exp\left(-4 \ln 2t^2/\tau_{\mathrm{FWHM}}^2\right), \tag{2}$$

where I_0 is the intensity of the measured pulse and τ_{FWHM} is the pulsewidth of the measured pulse. With Eqs. (1) and (2), the autocorrelation can be derived as

$$I_A(\tau) = I_0^2 \exp\left(-4 \ln 2t^2 \Big/ \left(\sqrt{2}\tau_{\mathrm{FWHM}}\right)^2\right). \tag{3}$$

The full-width at half-maximum (FWHM) is calculated by pulse shape; thus, the pulsewidth is counted by an exponential term. I_0 is normalized in the succeeding paragraphs. Compared with Eqs. (2) and (3), the width of autocorrelation in Eq. (3) is $\sqrt{2}\tau_{\mathrm{FWHM}}$.

When measuring the high-repetition-rate ultrashort pulse, time delay τ is easily changed and an autocorrelation curve is obtained. When the measured pulse is a single shot, time delay τ is generated by two wide beams that cross an angle. According to the principle of divided wavefronts, a beam is composed of many lines. When the beam arrives at the second-harmonic generation (SHG) crystal at a slanted angle, these lines impinge on the SHG crystal at different times. Given that two beams exist in autocorrelation, variable time delay τ is generated between these two bundles of lines. Figure 1 shows that when the angle between two beams is Φ and the length of the autocorrelation area in the x orientation is α, the maximum time delay of each side is

$$\tau_{\max}(x) = \alpha \sin(\Phi/2)/c. \tag{4}$$

c is velocity of light. Thus, the temporal window of the autocorrelator is $[-\tau_{\max}, \tau_{\max}]$.

Autocorrelation signals are symmetric in theory. However, asymmetric signals are sometimes obtained by experimentation. Therefore, the period

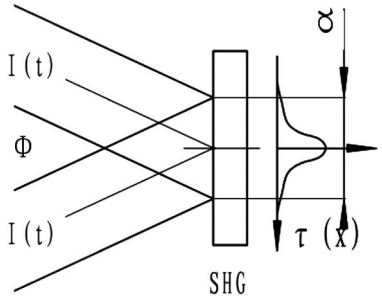

Fig. 1. Schematic of the single-shot autocorrelation: Φ is the angle between two beams, α is the length of the autocorrelation area, $\tau(x)$ denotes the time axis, and SHG is a crystal used to generate second-harmonic waves.

at which autocorrelation increases (rise slope) is not equal to the period at which it decreases (decline slope). In this study, an asymmetric factor σ is used to describe this phenomenon.

$$\sigma = \frac{\Delta\tau_r - \Delta\tau_f}{\Delta\tau_r + \Delta\tau_f} \times 100\%, \tag{5}$$

where $\Delta\tau_r$ is the FWHM of the autocorrelation's rise slope, which ranges from 50% to 100% of the peak value, and $\Delta\tau_f$ is the FWHM of the autocorrelation's decline slope, which ranges from 100% to 50% of the peak value. The width of autocorrelation $\Delta\tau_A$ (FWHM) is the sum of $\Delta\tau_r$ and $\Delta\tau_f$.

$$\Delta\tau_A = \Delta\tau_r + \Delta\tau_f. \tag{6}$$

Under this condition, the measured width $\Delta\tau_A$ of pulse autocorrelation has uncertainty δ with real width $\Delta\tau_0$.

$$\delta = \frac{\Delta\tau_A - \Delta\tau_0}{\Delta\tau_0} \times 100\%. \tag{7}$$

3. Analysis of the Near Field

We assume that a relationship exists between symmetric autocorrelation and measured pulse shape. For example, an asymmetric pulse can be described as

$$I(t) = \exp(-4 \ln 2t^2/\tau_{\mathrm{FWHM}}^2) + 0.5 \exp\left(-4 \ln 2(t+T)^2/\tau_{\mathrm{FWHM}}^2\right). \tag{8}$$

Its autocorrelation is

$$A(\tau) = \sqrt{\frac{\pi}{2}\frac{\tau_{\mathrm{FWHM}}^2}{4\ln 2}}\exp\left(-\frac{\tau^2}{\tau_{\mathrm{FWHM}}^2/2\ln 2}\right) + 0.5\sqrt{\frac{\pi}{2}\frac{\tau_{\mathrm{FWHM}}^2}{4\ln 2}}\exp\left(-\frac{(\tau-T)^2}{\tau_{\mathrm{FWHM}}^2/2\ln 2}\right) + 0.5\sqrt{\frac{\pi}{2}\frac{\tau_{\mathrm{FWHM}}^2}{4\ln 2}}\exp\left(-\frac{(\tau+T)^2}{\tau_{\mathrm{FWHM}}^2/2\ln 2}\right). \tag{9}$$

Distortion is observed in the rise and decline slopes if $T = \tau_{\mathrm{FWHM}}$ and $T = -\tau_{\mathrm{FWHM}}$, respectively. Figure 2 shows that the autocorrelation signal is symmetric even if the pulse shape is asymmetric. This result applies to any function and is widely used in signal processing systems. The asymmetry of autocorrelation is therefore not caused by distortion pulse shape, but by the nonideal autocorrelation process.

If the distribution of the measured pulse in its cross-section is uniform, the autocorrelation shape should be considered asymmetric. When the measured pulse is transmitted through many optical

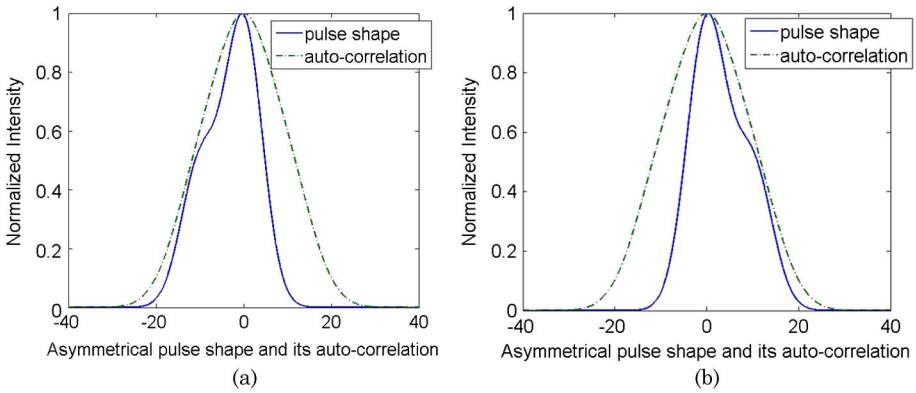

Fig. 2. (Color online) Asymmetric pulses and their autocorrelations: (a) distortion in rise slope ($T = \tau_{\mathrm{FWHM}}$) (b) distortion in decline slope ($T = -\tau_{\mathrm{FWHM}}$).

devices in a large laser facility, the near field, or its intensity distribution in its cross-section, becomes nonuniform because of damage on the gratings and nonuniformity of the very low sampling rate of larger optical devices [9,10]. In autocorrelation, two arms have the same times of reflections. Therefore, they have the same near field on the SHG crystal, indicating that high-intensity positions overlap in the near field and weak intensity positions are found at the same location. This phenomenon modulates $I_A(\tau)$ in Eq. (3), thereby causing the autocorrelation signal to be asymmetric. This problem is discussed by numerical simulation.

On the basis of the characteristics of a large laser facility, we can simplify near-field defects into two kinds in this analysis: linear variation and step variation. Each of these variations has two inverted orientations in the near field.

When the change in near-field distribution is a linear variation, a modulation function of intensity in the τ orientation can be described as

$$f_{\mathrm{linearI}}(\tau) = 0.5\tau/\tau_{\max} + 0.5, [-\tau_{\max}, \tau_{\max}]. \tag{10}$$

With this type I linear variation [Fig. 3(a)], the autocorrelation signal (3) is modulated on intensity I_0 of the pulse in Eq. (3). The signal on detectors is

$$I_{A,\mathrm{linearI}}(\tau) = I_A(\tau) \times f^2_{\mathrm{linear\ I}}(\tau). \tag{11}$$

Another modulation function of inverted intensity is

$$f_{\mathrm{linearII}}(\tau) = -0.5\tau \times \tau_{\max} + 0.5, [-\tau_{\max}, \tau_{\max}]. \tag{12}$$

With this type II linear variation [Fig. 3(a)], the autocorrelation signal on detectors is

$$I_{A,\mathrm{linearII}}(\tau) = I_A(\tau) \times f^2_{\mathrm{linearII}}(\tau). \tag{13}$$

When the change in near-field distribution is a step variation, a modulation function of intensity in the τ orientation is

$$f_{\mathrm{step\,I}}(\tau) = \begin{cases} 0.5, & [-\tau_{\max}, -0.1\tau_{\max}] \\ (0.5/0.2\tau_{\max}) \times \tau + 0.5, & [-0.1\tau_{\max}, 0.1\tau_{\max}] \\ 1, & [0.1\tau_{\max}, \tau_{\max}] \end{cases}. \tag{14}$$

With this type I step variation [Fig. 3(b)], the autocorrelation signal (3) becomes

$$I_{A,\mathrm{step\ I}}(\tau) = I_A(\tau) \times f^2_{\mathrm{step\ I}}(\tau). \tag{15}$$

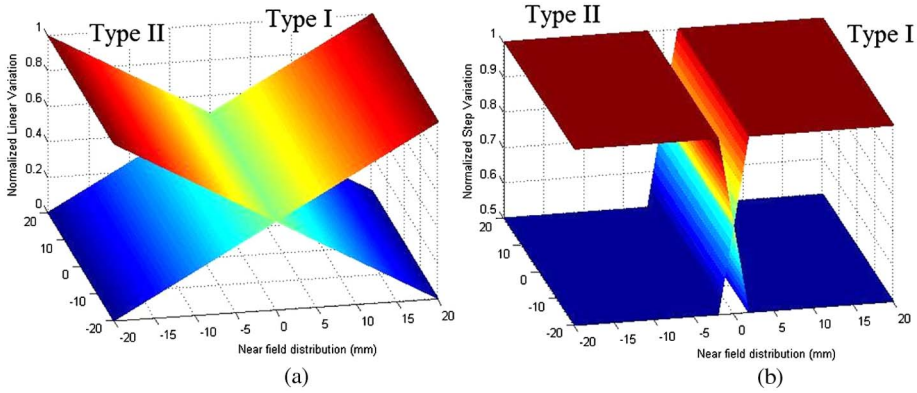

Fig. 3. (Color online) Autocorrelation aberration caused by the nonuniform distribution of the near field. (a) Linear variation of near-field distribution. (b) Step variation of near-field distribution.

Another modulation function of intensity in the τ orientation is

$$f_{\text{step II}}(\tau)=\begin{cases}1, & [-\tau_{\max},-0.1\tau_{\max}]\\ (-0.5/0.2\tau_{\max})\times\tau+1, & [-0.1\tau_{\max},0.1\tau_{\max}]\\ 0.5, & [0.1\tau_{\max},\tau_{\max}]\end{cases}. \tag{16}$$

With this type II step variation [Fig. 3(b)], the autocorrelation signal (3) is

$$I_{A,\text{step II}}(\tau)=I_A(\tau)\times f^2_{\text{step II}}(\tau). \tag{17}$$

From Eqs. (11), (13), (15), and (17), the simulation of signal asymmetry and measurement uncertainty from the near-field distribution can be derived (Table 1). In these calculations, if the pulsewidth of measured Gaussian pulse τ_{FWHM} is assumed to be 10 ps, then the width of autocorrelation $\sqrt{2}\tau_{\text{FWHM}}$ is 14.14 ps.

Table 1 shows that distorted pulses still cause symmetric autocorrelation because σ is zero. The asymmetric autocorrelation includes measurement uncertainty δ when σ is nonzero. Asymmetry σ from type I is negative, and that from type II is positive. They are equal in absolute value. Uncertainty δ from the rotation of types I and II are equal and both negative. Therefore, the pulsewidth of asymmetric autocorrelation signal $\Delta\tau_A$ is shorter than real width $\Delta\tau_0$.The asymmetry from linear variation is small ($\pm$2.11%), whereas that from step variation is large ($\pm$17.3%). The measurement uncertainty from linear variation is small (–6.36%), whereas that from step variation is large (–42.2%).

4. Analysis of Focal Lines

In some autocorrelators, cylindrical lenses are used to generate focal lines, which can improve the efficiency of SHG [11,12]. These two focal lines may be mismatched and do not overlap exactly, as shown in Fig. 4. This case is possible in measuring petawatt laser pulses because of the difficulty in adjustment. A modulation function of type I in Fig. 4(a) in the time t orientation can be described as

$$f_{\text{rotationI}}(\tau)=\begin{cases}0, & [-\tau_{\max},\tau_{\text{start}}]\\ \left(\dfrac{\tau-\tau_{\text{start}}}{\tau_{\text{eff}}}\right)^2, & [\tau_{\text{start}},\tau_{\max}]\end{cases}. \tag{18}$$

In this function, the initiation of modulation is $\tau_{\text{start}}=\tau_{\max}-k\times 2\tau_{\max}$, and the length of the converted effective area in the x orientation into temporal scale is $\tau_{\text{eff}}=k\times 2\tau_{\max}$. $k=1.0\sim 0$ is used to describe the severity of the rotation, where $k=1.0$ indicates that the two beams overlap exactly, whereas $k=0$ means the beams do not overlap. With this rotation, the autocorrelation signal (3) becomes

$$I_{A,\text{rotationI}}(\tau)=I_A(\tau)\times f^2_{\text{rotationI}}(\tau). \tag{19}$$

Another modulation function of type II in Fig. 4(b) is

$$f_{\text{rotation II}}(\tau)=\begin{cases}\left(\dfrac{\tau_{\text{end}}-\tau}{\tau_{\text{eff}}}\right)^2, & [-\tau_{\max},\tau_{\text{end}}]\\ 0, & [\tau_{\text{end}},\tau_{\max}]\end{cases}. \tag{20}$$

In this function, the termination of modulation is $\tau_{\text{end}}=-\tau_{\max}+k\times 2\tau_{\max}$, and the length of the converted effective area in the x orientation into temporal scale is $\tau_{\text{eff}}=k\times 2\tau_{\max}$. The corresponding autocorrelation signal (3) becomes

$$I_{A,\text{rotationII}}(\tau)=I_A(\tau)\times f^2_{\text{rotationII}}(\tau). \tag{21}$$

Asymmetry and uncertainty from the rotated focal lines can be derived using Eqs. (19) and (21) [Fig. 4(c)].

Figure 4(c) shows that asymmetry σ from type I rotation is negative, and that from type II rotation is positive. They are equal in absolute value. However, uncertainty δ from the rotations of types I and II are equal and both negative. Therefore, the pulse width of asymmetric autocorrelation signal $\Delta\tau_A$ is also shorter than real width $\Delta\tau_0$. The absolute values of asymmetry from rotations are ranged from 2.21% to 5.85%. They are greater than absolute value of linear variation ($\pm$2.11%) and smaller than that of step variation ($\pm$17.3%). And measurement uncertainties range from –10.3% to –32.3%. They are between uncertainty of linear variation (–6.36%) and that of step variation (–42.2%).

When cylindrical lenses are used, asymmetry and uncertainty also occur because of the mismatch between the two focal lines. Beam alignment and

Table 1. Asymmetry and Uncertainty from Near-Field Distribution

Distortion of pulse or nonideal autocorrelation	$\Delta\tau_0$ ps	$\Delta\tau_A$ ps	$\Delta\tau_r$ ps	$\Delta\tau_f$ ps	σ	δ
Distortion in rise slope	/	23.56	11.78	11.78	0	/
Distortion in decline slope	/	23.56	11.78	11.78	0	/
Linear variation, type I	14.14	13.24	6.48	6.76	–2.11%	–6.36%
Linear variation, type II	14.14	13.24	6.76	6.48	2.11%	–6.36%
Step variation, type I	14.14	8.17	3.38	4.79	–17.3%	–42.2%
Step variation, type II	14.14	8.17	4.79	3.38	17.3%	–42.2%

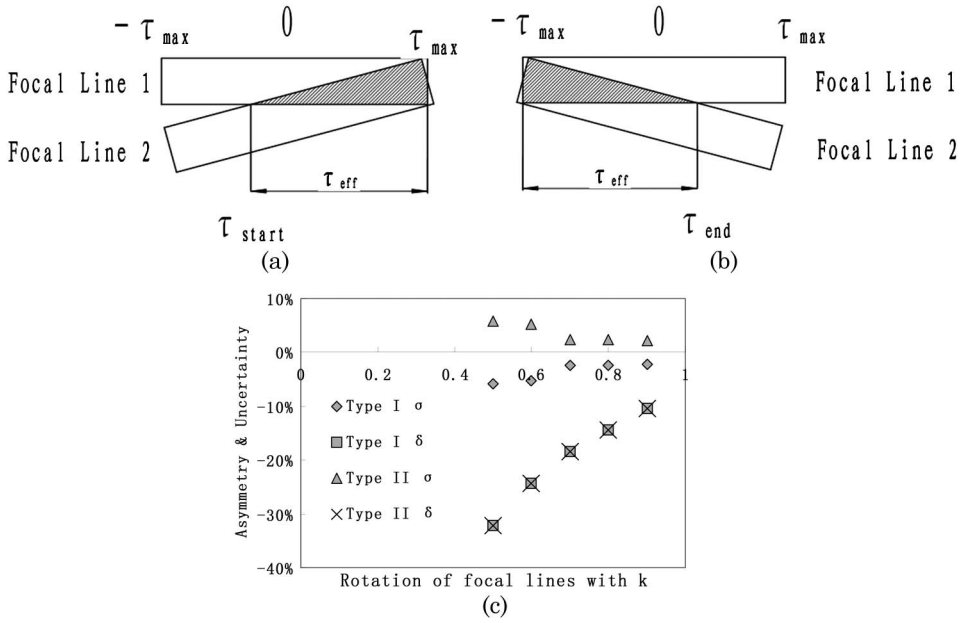

Fig. 4. Autocorrelation aberration caused by the rotation aberration of two arms (a) Rotation of type I in autocorrelation arms; (b) Rotation of type II in autocorrelation arms; (c) Asymmetry and uncertainty from rotation.

aim require precise adjustment, which is difficult for sampling the large-energy, single-shot petawatt laser pulses.

5. Analysis of Mixture

As seen in Table 1, asymmetry σ from type I is equal to that from type II in absolute value. If the two arms of the autocorrelator are separately transmitted through even and odd reflectors, the near-field distribution of the two arms on the SHG crystal is mirror imaged. This mirror imaging can generate a symmetric signal and reduce uncertainty (Table 2). Asymmetry σ becomes zero, and uncertainty δ is −4.53% for linear variation and −12.3% for step variation. Measurement data was obtained with a little uncertainty and becomes more precise.

For a step variation, uncertainty is greater than that of linear variation. The simulation of a mixture of step variation and rotation of the focal lines are analyzed (Fig. 5). Case 1 is a mixture of type I step variation and type I rotation, denoted as mixI. Case 2 is a mixture of type II step variation and type I rotation, labeled mixII. Case 3 is a mixture of type I step variation and type II rotation, designated as mixIII. Case 4 is a mixture of type II step variation and type II rotation, called mixIV.

Figure 5(a) shows that asymmetry σ is reduced when k changes from 0.9 to 0.5, a reduction that leads to shorter rise and decline slopes that can yield a smaller σ. Disregarding this small σ may mistakenly show that the measurement has little uncertainty. The absolute values of mixII and mixIII are greater than those of mixI and mixIV when k is above 0.7. This phenomena means high-intensity positions can generate much more asymmetry than weak-intensity positions when mismatch is small. Absolute values of these four cases are closed to that of rotations in Fig. 4 (±5.85%) when k is below 0.7. This phenomena means these four cases are similar with Fig. 4 because effective area becomes uniform. However, σ will not be zero even if k is 0.2 in our simulation. As seen in Fig. 5(b), uncertainty δ increases when k varies from 0.9 to 0.5. The uncertainty of these four cases becomes equal when k is below 0.7.

6. Experimental Results

The autocorrelation system in the experiments is shown in Fig. 6. The measured pulse impinges on a beam splitter and is then divided into two arms. The transmitted arm impinges on mirror M_1 and goes through a cylindrical lens (CL_1). The reflected arm goes through a time delay composed of M_2, M_3, and is then guided into a cylindrical lens (CL_2) by M_4. These two arms are overlapped on SHG crystal beta-barium borate via the mirror image technique. The autocorrelation signal is coupled with the fiber array detector using an imaging system composed of two

Table 2. Asymmetry and Uncertainty from Mirror Image

Distortion of pulse or nonideal autocorrelation	$\Delta\tau_0$ ps	$\Delta\tau_A$ ps	$\Delta\tau_r$ ps	$\Delta\tau_f$ ps	σ	δ
Linear variation of mirror image	14.14	13.5	6.76	6.76	0	−4.53%
Step variation of mirror image	14.14	12.4	6.20	6.20	0	−12.3%
Experimental data with lenses in Fig. 6	/	4.13	1.75	2.39	−15.5%	/
Experimental data without lenses in Fig. 6	/	7.80	3.90	3.90	0	≤ − 12.3%

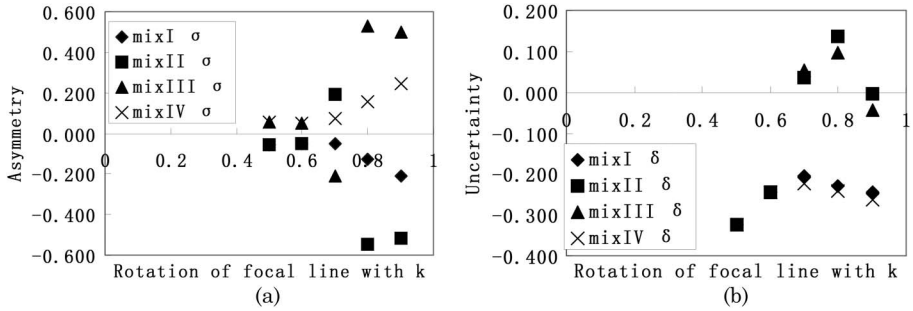

Fig. 5. Asymmetry and uncertainty of the mixture of step variation and rotation (a) Asymmetry of mixture of step variation and rotation; (b) Uncertainty of mixture of step variation and rotation.

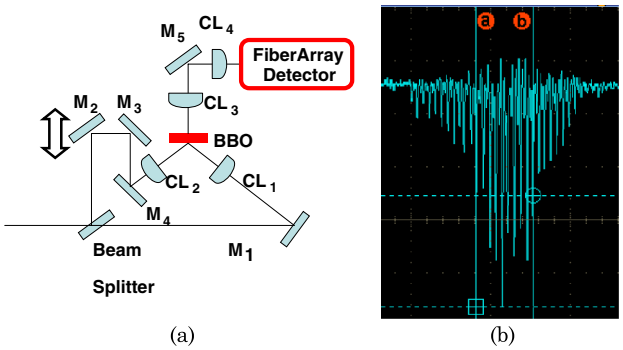

Fig. 6. (Color online) Autocorrelation aberration in experiments. (a) Autocorrelator of SGII-PW: M_1, M_2, M_3, M_4, M_5, are mirrors; CL_1, CL_2, CL_3, CL_4 are cylindrical lenses. (b) Measured experimental data on the intensity of autocorrelation curves at large-energy, single-shot measurement of SGII petawatt laser pulses.

cylindrical lenses (CL_3, CL_4). The autocorrelator requires precise adjustment because it contains three lenses, which are removed in subsequent experiments.

Examples of experimental data are analyzed in this manner (Table 2). The data derived by the autocorrelator with the lenses show that asymmetric factor σ is −31% at a pulsewidth of 4.13 ps. This uncertainty is caused only by the rotation aberration of two focal lines when the mirror image technique is adopted. We can also conclude that rotation factor k is higher than 0.5, and uncertainty δ is greater than −30%. The data obtained by the autocorrelator without the lenses show that asymmetric factor σ is zero, and uncertainty δ is less than −12.3% compared with the variation derived by mirror imaging.

7. Conclusion

The asymmetry of autocorrelation causes uncertainty in pulsewidth measurement. The pulsewidth of an asymmetric autocorrelation signal $\Delta\tau_A$ is shorter than real width $\Delta\tau_0$. Different methods can be used to reduce uncertainty and improve accuracy. Uniform distribution in the near field is required to avoid asymmetric autocorrelation signals. Linear variation is better than step variation in terms of near-field distribution. The two arms of an autocorrelator can be separately transmitted through even and odd reflectors, thereby obtaining mirror images on an SHG crystal. Beam area can be increased to simplify the requirements for beam alignment and aim, avoiding a mismatch of the focal lines in autocorrelation. Even measured pulses can be guided onto the SHG crystal without a lens because the intensity of picosecond pulses is sufficiently high for pulsewidth measurement.

The authors thank Prof. Jian Zhu, Prof. Yuxin Leng, and Prof. Guang Xu for the discussion.

References

1. I. N. Ross, D. Karadia, and J. M. Barr, "Single shot measurement of pulse duration for a picosecond pulse at 249 nm," Appl. Opt. **28**, 4054–4056 (1989).
2. J. Collier, C. Danson, C. Johnson, and C. Mistry, "Uniaxial single shot autocorrelator," Rev. Sci. Instrum. **70**, 1599–1602 (1999).
3. K. Oba, P.-C. Sun, Y. T. Mazurenko, and Y. Fainman, "Femtosecond single-shot correlation system: a time-domain approach," Appl. Opt. **38**, 3810–3817 (1999).
4. Z. Sack and G. Mourou, "Adjusting pulse-front tilt and pulse duration by use of a single-shot autocorrelator," Opt. Lett. **26**, 462–464 (2001).
5. X. Ouyang, X. Li, Y. Zhang, Z. Li, G. Xu, T. Wang, B. Zhu, and J. Zhu, "A method to obtain pulse contrast on a single shot," Chin. Opt. Lett. **7**, 1001–1003 (2009).
6. F. Zhang, X. Ouyang, M. Sun, Q. Bi, X. Xie, and Z. Lin, "Diffraction grating single-shot correlation system for measurement of picosecond laser pulses," Chin. Opt. Lett. **8**, 1053–1056 (2010).
7. S. Tang, X. Ouyang, L. Ji, C. Liu, Y. Zhang, X. Li, K. Huang, B. Zhu, J. Zhu, and Z. Lin, "Phase mismatching analysis of third-harmonic generation in BBO crystal," Chin. Opt. Lett. **8**, 612–614 (2010).
8. J. Ma, P. Yuan, Y. Wang, D. Zhang, H. Zhu, and L. Qian, "Single-shot cross-correlator using a long-wavelength sampling pulse," Opt. Lett. **36**, 978–980 (2011).
9. Z. Lin, X. He, and J. Zhu, "Laser fusion driver development in SIOM and some related optical technology progress in China," in *Conference on Lasers and Electro-Optics/Pacific Rim (CLEO/PR)* (Optical Society of America, 2007), paper MA1_1.
10. C. A. Haynam, P. J. Wegner, J. M. Auerbach, M. W. Bowers, S. N. Dixit, G. V. Erbert, G. M. Heestand, M. A. Henesian, M. R. Hermann, K. S. Jancaitis, K. R. Manes, C. D. Marshall, N. C. Mehta, J. Menapace, E. Moses, J. R. Murray, M. C. Nostrand, C. D. Orth, R. Patterson, R. A. Sacks, M. J. Shaw, M. Spaeth, S. B. Sutton, W. H. Williams, C. C. Widmayer, R. K. White, S. T. Yang, and B. M. Van Wonterghem, "National Ignition Facility laser performance status," Appl. Opt. **46**, 3276–3303 (2007).
11. P. Simon, H. Gerhardt, and S. Szatmarl, "A single-shot autocorrelator for UV femtosecond pulse," Meas. Sci. Technol. **1**, 637–639 (1990).
12. P. Bowlan and R. Trebino, "Complete single-shot measurement of arbitrary nanosecond laser pulses in time," Opt. Express **19**, 1367–1377 (2011).